

See discussions, stats, and author profiles for this publication at: <https://www.researchgate.net/publication/275256174>

# Conjugation-Break Spacers in Semiconducting Polymers: Impact on Polymer Processability and Charge Transport Properties

ARTICLE in MACROMOLECULES · APRIL 2015

Impact Factor: 5.8 · DOI: 10.1021/acs.macromol.5b00194

---

CITATIONS

3

READS

47

## 6 AUTHORS, INCLUDING:



[Yaping Zang](#)

Chinese Academy of Sciences

13 PUBLICATIONS 56 CITATIONS

[SEE PROFILE](#)



[Chong-an Di](#)

Chinese Academy of Sciences

109 PUBLICATIONS 3,741 CITATIONS

[SEE PROFILE](#)



[Jianguo Mei](#)

Purdue University

40 PUBLICATIONS 2,750 CITATIONS

[SEE PROFILE](#)

## Conjugation-Break Spacers in Semiconducting Polymers: Impact on Polymer Processability and Charge Transport Properties

Yan Zhao,<sup>†</sup> Xikang Zhao,<sup>†</sup> Yaping Zang,<sup>‡</sup> Chong-an Di,<sup>‡</sup> Ying Diao,<sup>§</sup> and Jianguo Mei<sup>\*,†,||</sup>

<sup>†</sup>Department of Chemistry, Purdue University, 560 Oval Drive, West Lafayette, Indiana 47907, United States

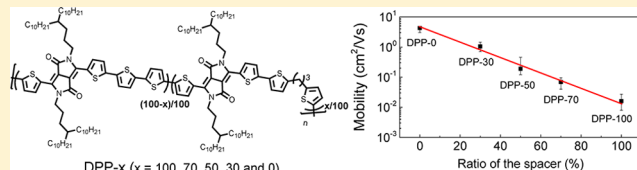
<sup>‡</sup>Key Laboratory of Organic Solids, Institute of Chemistry, Chinese Academy of Sciences, Beijing 100190, China

<sup>§</sup>Department of Chemical & Biomolecular Engineering, University of Illinois at Urbana-Champaign, 600 South Mathews Avenue, Urbana, Illinois 61801, United States

<sup>||</sup>Birck Nanotechnology Center, Purdue University, 1205 W. State St., West Lafayette, Indiana 47906, United States

### S Supporting Information

**ABSTRACT:** Conjugation-break spacers (CBSs) are intentionally introduced into the diketopyrrolopyrrole (DPP)-based polymer backbones. We reveal that the solution processability progressively increases with the percentage of CBSs, while charge mobility inversely varies to the CBS ratio. For instance, the polymer DPP-30 with solubility of ~10 mg/mL in dichlorobenzene provides an average mobility over  $1.4 \text{ cm}^2 \text{ V}^{-1} \text{ s}^{-1}$ , while DPP-0 exhibits an average mobility of  $4.3 \text{ cm}^2 \text{ V}^{-1} \text{ s}^{-1}$  with solubility of ~3 mg/mL. This correlation provides a general guidance to design polymers with desired electronic performance and solution processability for large-scale roll-to-roll processing. Most encouraging, DPP-70 can be melt processed in air and provide hole mobilities up to  $0.30 \text{ cm}^2 \text{ V}^{-1} \text{ s}^{-1}$ , substantially higher value than their solution-processed counterparts about  $0.1 \text{ cm}^2 \text{ V}^{-1} \text{ s}^{-1}$ . The mobility boost in melt-processed devices, together with completely eliminating the need to use toxic solvent in the processing, encourages to design melt-processable polymers for electronic devices.



## INTRODUCTION

Conjugated polymers are promising optoelectronic materials for next-generation flexible and printed electronics.<sup>1–4</sup> Extensive efforts have been put into the design and synthesis of conjugated polymers.<sup>5–11</sup> A plethora of knowledge about how to rationally control their optical, electronic, and redox properties has been realized in the development of numerous conjugated polymers.<sup>12–15</sup> In contrast, partially conjugated semiconducting polymers with intentionally placed, non-conjugated flexible linkages along the polymer backbones have received little attention.<sup>16,17</sup> There are two primary reasons. First, flexible linkages create high degrees of conformational and energetic disorder in polymer chains. Second, conjugation-break spacers (CBSs) disrupt the extended  $\pi$ -electron delocalization along polymer backbones. In principle, both factors can have a negative influence on electronic properties, particularly for charge transport.<sup>17,18</sup> On the other hand, high performance conjugated polymers are often plagued with poor solution processability, a leading factor for batch-to-batch variations in both polymer synthesis and device fabrication.<sup>19,20</sup> This limits applications of conjugated polymers in large-scale flexible electronics. Conventionally, tuning solution processability of polymers in organic solvents can be achieved by changing the size and shape of flexible solubilizing chains attached to polymer backbones.<sup>21</sup> However, the modulation of polymer solution processability and electronic performance turns out to be nontrivial. In this study, we report

a different strategy to address this problem, which is to introduce flexible CBSs into conjugated backbones. This strategy not only provides a facile approach to modulate solution processability of the polymers but also unexpectedly offers a promising strategy to prepare melt-processable semiconducting polymers. The former would make solution processing more controllable. The latter could potentially eliminate the need for toxic organic solvents for thin-film formation, which would have a positive impact on both economic and environmental aspects. Understanding charge transport in disordered polymer films is considered to be the grand challenge in the field, as it plays a crucial role in next-generation semiconducting polymer design and process. Different theoretical models are proposed to describe charge transport in polymer thin films.<sup>18,22–24</sup> Our approach provides a new platform for fundamental studies on charge transport from a different perspective.

## RESULTS AND DISCUSSION

**Synthesis and Physical Properties Characterization.** Diketopyrrolopyrrole (DPP)-based semiconducting polymers have been extensively investigated for their charge transport properties.<sup>25</sup> In this study, we choose the previously reported

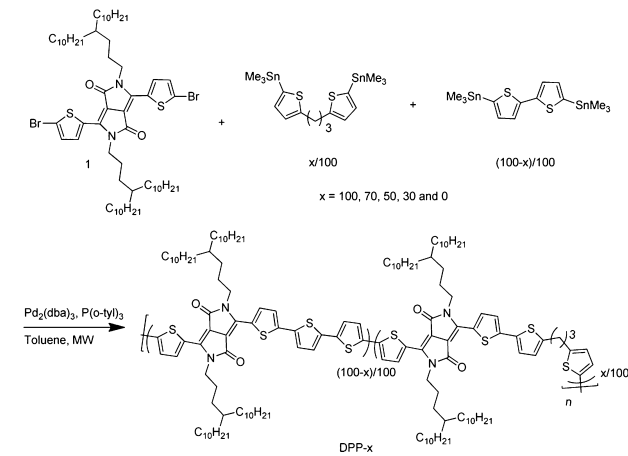
Received: January 28, 2015

Revised: March 17, 2015

Published: April 1, 2015

diketopyrrolopyrrole–quaterthiophene copolymer as the parent polymer and the propyl unit as the flexible CBS.<sup>26</sup> The synthetic route for the DPP polymers is shown in Scheme 1. The synthetic details for monomers and polymers can be found in the Supporting Information, and their physical characterization data are summarized in Table 1.

**Scheme 1. Synthetic Route for DPP- $\alpha$  Polymers**



The ratio of the CBS is varied from 100%, 70%, 50%, 30% to 0%, namely from being fully flexible (DPP-100) to being fully rigid (DPP-0). The incorporation of propyl linkage was confirmed by monitoring the ratio between the proton ( $CH_2$ ) next to thiophene ring (~2.9 ppm) and the proton ( $CH_2$ ) next to nitrogen atom (~4.0 ppm) in a nuclear magnetic resonance (NMR) study (see Figure S1, Supporting Information). The number-average molar mass and polydispersity were evaluated by high temperature gel permeation chromatography (GPC) using trichlorobenzene as the eluent at 180 °C and polystyrene for calibration (see Figure S2, Supporting Information). The number-average molecular weights are 30.7, 23.0, 19.5, 16.9, and 12.5 kDa for DPP-0, DPP-30, DPP-50, DPP-70 and DPP-100, with the polydispersities of 3.61, 3.24, 2.60, 2.20, and 1.98, respectively. The difference in molecular weights for this set of polymers can be explained by the degree of deviation from the random-coil model, which is the basis for the universal calibration in the GPC measurement.<sup>27</sup> The fewer CBSs a polymer contains, the more we expect a derivation from the random-coil model for the polymers. Additionally, extended conjugation along polymer backbone will cause aggregation among polymer chains and hence lead to the exaggeration of molecular weights. The more extended conjugation along the polymer backbone is

present, and the higher degree of aggregation is expected in polymer solution. Therefore, the direct comparison of molecular weights is challenging among this set of polymers.

The thermal stability for DPP polymers was evaluated by thermal gravimetric analysis (TGA). The decomposition temperatures are in the range of 390–400 °C (Figure S3). Based on the weight loss information, it is believed that the decomposition starts from the loss of alkyl chains on the nitrogen atoms. Differential scanning calorimetry (DSC) analysis was carried out to obtain phase transition information (see Figure S4, Supporting Information). No noticeable thermal transition is observed in the range from 100 to 350 °C for DPP-0, DPP-30, and DPP-50, while DPP-70 and DPP-100 exhibit melting transitions around 270 and 180 °C in the first scan, respectively. The melting transitions of DPP-70 and DPP-100 are not reversible even with a scanning rate as low as 1 °C/min. Upon heated and cooled on a hot plate, however, the polymers exhibit a reversible phenomenon of liquidation and solidification, as shown in Figure S4. In the present study, we took the advantage of this phenomenon and demonstrated a solventless process for the fabrication of field-effect transistors.

The solution and solid-state UV–vis–NIR spectra of DPP polymers reveal the impact of propyl CBS on the optical properties, as summarized in Table 1. A bathochromic shift is observed in both dichlorobenzene solutions and thin films for this set of polymers (Figure 1) due to the extension of

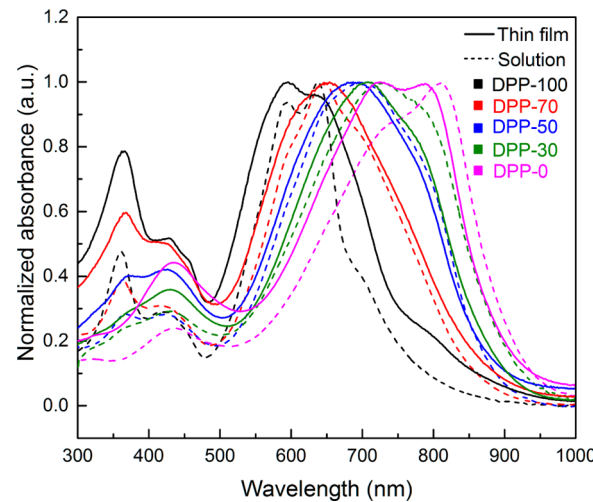


**Figure 1.** UV–vis–NIR spectra of DPP-100, DPP-70, DPP-50, DPP-30, and DPP-0 in solutions (dot) and as thin films (solid).

conjugation along the polymer backbone from DPP-100 to DPP-0. From solution to thin film, DPP-0, DPP-30, and DPP-

**Table 1. Physical Properties of DPP Polymers**

$M_n$ (kDa)/PDI <sup>a</sup>	$T_d$ <sup>b</sup> (°C)	$T_m$ <sup>c</sup> (°C)	$\lambda_{\max}^{\text{abs}}$ (nm)		$\lambda_{\text{onset}}^{\text{abs}}$ (nm) film <sup>e</sup>	$E_g^{\text{opt},f}$ (eV)	energy levels (eV)	
			solution <sup>d</sup>	film <sup>e</sup>			$E_{\text{HOMO}}^g$	$E_{\text{LUMO}}^h$
DPP-0	30.7/3.61	400	740, 811	725, 789	937	1.32	-4.97	-3.65
DPP-30	23.0/3.24	400	729	708	925	1.34	-5.01	-3.67
DPP-50	19.5/2.60	399	699	687	915	1.36	-5.08	-3.72
DPP-70	16.9/2.20	395	270, 180	645	654	1.37	-5.09	-3.72
DPP-100	12.5/1.98	390	180	594, 638	595, 637	1.40	-5.13	-3.73

<sup>a</sup>Trichlorobenzene as the eluent at 180 °C. <sup>b</sup>Decomposition temperature. <sup>c</sup>Melting temperature. <sup>d</sup>In dichlorobenzene solution. <sup>e</sup>Spin-coated films on glass substrates, annealed at 150 °C. <sup>f</sup>Calculated from the onset absorption  $E_g^{\text{opt}} = 1240/\lambda_{\text{onset}}^{\text{abs}}$  (nm). <sup>g</sup>Obtained from UPS. <sup>h</sup>Calculated using the equation  $E_{\text{LUMO}} = E_{\text{HOMO}} + E_g^{\text{opt}}$ .

Table 2. Field-Effect Performance Characteristics of OFETs Fabricated by Different Processing Methods

	spin coating				drop casting				melt processing			
	$\mu_{\text{max}}$ (cm <sup>2</sup> /(V s))	$\mu_{\text{avg}}$ (cm <sup>2</sup> /(V s))	V <sub>Th</sub> (V)	I <sub>on</sub> /I <sub>off</sub>	$\mu_{\text{max}}$ (cm <sup>2</sup> /(V s))	$\mu_{\text{avg}}$ (cm <sup>2</sup> /(V s))	V <sub>Th</sub> (V)	I <sub>on</sub> /I <sub>off</sub>	$\mu_{\text{max}}$ (cm <sup>2</sup> /(V s))	$\mu_{\text{avg}}$ (cm <sup>2</sup> /(V s))	V <sub>Th</sub> (V)	I <sub>on</sub> /I <sub>off</sub>
DPP-0	4.27	3.52	-4.9	~10 <sup>6</sup>	4.85	4.28	-4.3	~10 <sup>6</sup>				
DPP-30	1.43	0.91	-4.3	~10 <sup>6</sup>	1.44	1.05	-4.6	~10 <sup>6</sup>				
DPP-50	0.44	0.27	-5.5	~10 <sup>5</sup>	0.46	0.19	-6.1	~10 <sup>5</sup>				
DPP-70	0.091	0.065	-7.9	~10 <sup>5</sup>	0.095	0.069	-7.4	~10 <sup>5</sup>	0.30	0.21	-4.3	~10 <sup>5</sup>
DPP-100	0.026	0.014	-9.2	~10 <sup>4</sup>	0.027	0.016	-8.6	~10 <sup>5</sup>	0.045	0.032	-4.5	~10 <sup>5</sup>

50 exhibit a clear hypochromic shift, whereas DPP-70 and DPP-100 show a limited bathochromic shift with an obvious spectral broadening. It is noted that a broad absorption emerges around 800 nm in the DPP-100 thin film, indicating the formation of strong excitonic interactions and the formation of  $\pi$ -stacks. The presence of  $\pi$ -stacks is supported by atomic force microscope (AFM) and grazing incidence X-ray diffraction (GIXRD) studies in the following section. The HOMO energy levels of the polymers are in the range of -4.97 and -5.13 eV, estimated by ultraviolet photoemission spectroscopy (UPS) and shown in Table 1. The difference in the HOMO levels for DPP-0 and DPP-100 is about 0.16 eV, and the difference is even smaller for the LUMO energy levels, only about 0.08 eV. It suggests that the LUMO level is more localized in a good agreement with the theoretical calculation.<sup>28</sup>

**Polymer Processability and Charge Transport Properties.** The introduction of CBSs into conjugated backbones improves polymer solution processability as a result of disrupting of backbone rigidity and inducing higher conformational freedom in solution. Indeed, the solubilities of these polymers in common organic solvents progressively increase with the percentage of CBSs. For instance, DPP-30 exhibits much improved solubility in dichlorobenzene about ~10 mg/mL, in comparison with that of DPP-0 (~3 mg/mL). Fully flexible DPP-100 shows solubility greater than 50 mg/mL under the same conditions. On the other hand, it is understood that the gain in solubility will be accompanied by the loss in charge transport performance because the presence of CBSs disrupts the efficient intrachain charge transport pathway.

To investigate the influence of CBSs on the charge transport properties of these polymers, bottom-gate, bottom-contact (BGBC, see Supporting Information Figure S5a) organic field-effect transistors (OFETs) were fabricated with silicon wafers as the back gate electrode, a 300 nm thermally oxidized SiO<sub>2</sub> layer as the gate dielectric, and prepatterned gold electrodes as the source/drain. Passivation of the SiO<sub>2</sub> layer was achieved by treating its surface with octadecyltrichlorosilane (OTS). Details of OFET fabrication, measurement, and calculation can be found in the Supporting Information. All mobility values reported here were conservatively extracted from the electrical characteristics to ensure a fair assessment. In addition, our device studies were independently reproduced and validated by another research group (see Supporting Information Table S1). Spin-coated, drop-cast, and melt-processed OFETs were fabricated and optimized. The device characteristics are summarized in Table 2. For devices fabricated by spin coating from dichlorobenzene solution and annealed in vacuum at 150 °C, DPP-0 exhibited the maximum hole mobility of 4.27 cm<sup>2</sup> V<sup>-1</sup> s<sup>-1</sup>, with an average mobility of 3.52 cm<sup>2</sup> V<sup>-1</sup> s<sup>-1</sup>. These results are in line with other reported DPP-based OFETs.<sup>25,26</sup> With 30% CBSs along the polymer backbone, DPP-30 surprisingly presented the mobility up to 1.43 cm<sup>2</sup> V<sup>-1</sup> s<sup>-1</sup>

over the benchmark value (1 cm<sup>2</sup> V<sup>-1</sup> s<sup>-1</sup>) for high performance polymers. The representative transfer and output curves of DPP-30 are shown in Figure 2a,b. With the increasing

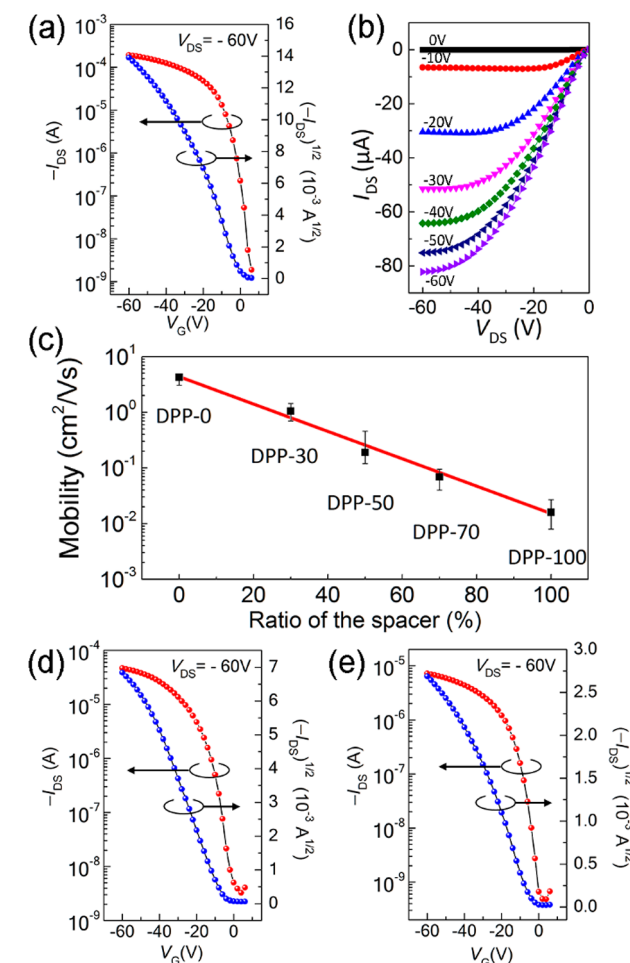


**Figure 2.** (a, b) Representative transfer and output characteristics of OFETs fabricated by spin coating based on polymer DPP-30. (c) Correlation between the mobility and the CBS ratio of these five polymers. (d, e) Transfer characteristics of melt-processed OFETs for DPP-70 and DPP-100, respectively. Over 100 devices were tested and calculated for each polymer. The channel length is 30  $\mu$ m, and the channel width is 1000  $\mu$ m for all devices.

of CBSs in the polymer backbone, charge carrier mobilities of DPP-50, DPP-70, and DPP-100 predictably fell (see Figures S6–S8). With over 100 devices for each polymer measured, we found that the logarithmic mobility is almost proportional to the CBS ratio in an inverse manner, as shown in Figure 2c. In conjunction with the solubility improvement, we demonstrate that polymer mobility and solubility could be modulated

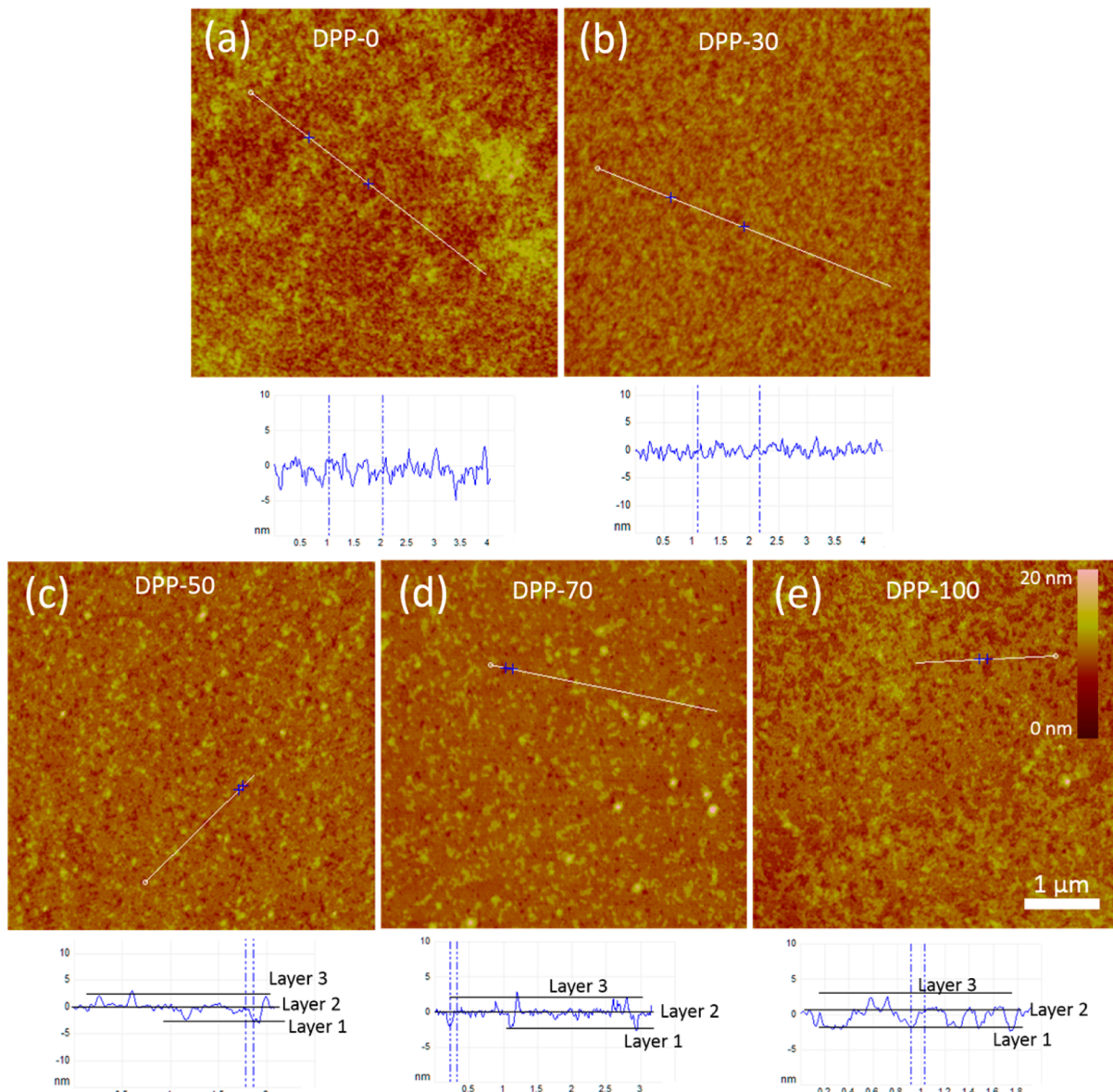


**Figure 3.** AFM images of spin-coated DPP thin films. The polymer thin films were fabricated by spin coating on OTS modified Si/SiO<sub>2</sub> substrates. The annealing temperature was 150 °C.

through the introduction of CBSs. In other words, a fine balance between performance and processability can be reached based on needs. The present approach of introducing CBSs into semiconducting polymers will likely play a significant role in practical applications. Drop-cast devices provided similar results, as shown in Table 2. Annealing of the devices at 150 °C in air on a hot plate was also carried out. The results listed in Supporting Information Table S2 indicate that the transistor devices have excellent thermal stability in air.

From the previous DSC study, we learned that melting transitions exist in DPP-70 and DPP-100. We also knew the devices were stable in air from the annealing study. We hence speculated that these polymers might be suitable for the melt processing, which is currently widely practiced for making plastic thin films in industry. We fabricated the melt-processed OFETs by directly placing DPP-70 and DPP-100 solids on the prepatterned, OTS-treated silicon wafer, which was then subjected to 250 and 200 °C in air (with/without nitrogen flow protection), respectively (see Supporting Information

Figure S5b). OFET transfer curves are shown in Figure 2d,e and Supporting Information Figures S9 and S10, and performance characteristics are summarized in Table 2 and Table S3. The mobilities are as high as 0.30 and 0.045 cm<sup>2</sup> V<sup>-1</sup> s<sup>-1</sup> for DPP-70 and DPP-100, which are 2 or 3 times of the ones processed through solution processing. To the best of our knowledge, this is the first case that meaningful OFETs are fabricated via melt processing. Compared to intensively investigated solution processing methods, melt processing completely eliminates the need of using toxic organic solvents.

**AFM and GIXRD Studies.** To understand the correlation between microstructure and transistor performance, atomic force microscope (AFM) and grazing incidence X-ray diffraction (GIXRD) studies were performed on both spin-coated and melt-processed thin films on OTS-covered Si/SiO<sub>2</sub> substrates. The AFM study illustrates that DPP-0 exhibits fibril-like microstructures across the thin film, commonly observed in conjugated polymers and shown in Figure 3. This is because conjugated polymers have rigid-rod-like backbones. The intense

$\pi-\pi$  interaction of conjugation planes drove the crystallization and formed 1-D nanofibril aggregates with large aspect ratios. In contrast, DPP-100 presents 2-D lamellar microstructures across the spin-coated films. Each layer is about  $\sim 2.2\text{--}2.4$  nm thick, which is close to the lamellar spacing for the polymers observed by GIXRD. Lamellar microstructures are often found in highly crystalline small molecule thin films but rarely observed in donor–acceptor type semiconducting polymer thin films.<sup>16</sup> This observation suggests DPP-100 may resemble small molecules in a way that high crystallinity is preserved. This is clearly resulted from the presence of flexible spacer along the polymer backbone. The thin film morphology of DPP-30 resembles more like that of DPP-0, while DPP-50 and DPP-70 present microstructures similar to DPP-100. Overall, the thin films gradually transition from fibril-like textures to lamellar textures with the addition of flexible spacer along the polymer backbones.

The GIXRD measurements reveal that all spin-coated polymer thin films exhibit a dominant edge-on  $\pi-\pi$  stacking, favorable for charge transport. With the presence of the CBS, the full width at half-maximum (fwhm) of both the lamellar and  $\pi-\pi$  stacking peaks in spin-coated films is reduced by approximately 25% from DPP-0 to DPP-100 (Table 3). This

**Table 3. Crystallographic Parameters for the Spin-Coated DPP Polymer Films by GIXRD**

	DPP-0	DPP-30	DPP-50	DPP-70	DPP-100
lamella spacing ( $\text{\AA}$ )	22.28	22.07	21.96	21.75	21.64
lamella peak fwhm ( $1/\text{\AA}$ )	0.044	0.038	0.039	0.041	0.035
$\pi-\pi$ stacking distance ( $\text{\AA}$ )	3.62	3.64	3.65	3.65	3.62
$\pi-\pi$ peak fwhm ( $1/\text{\AA}$ )	0.084	0.078	0.087	0.076	0.063

indicates that the crystalline domains become more ordered from DPP-0 to DPP-100, in line with the AFM observations.<sup>29</sup> Application of Scherrer analysis on the lamellar stacking peaks yields the apparent crystalline domain coherent length of 14 and 18 nm for DPP-0 and DPP-100, respectively. In addition, the lamellar stacking distance decreases from 22.28  $\text{\AA}$  for DPP-0 to 21.64  $\text{\AA}$  for DPP-100, which could be due to closer alkyl chain stacking with increased molecular ordering. All the information suggests that DPP-100 thin film exhibit much larger domains or significantly improved ordering within the domain, in comparison with DPP-0 thin film. DPP-30, DPP-50, and DPP-70 have irregular polymer backbones with statistically distributed CBSs. The complexity of backbone arrangements has surprisingly not introduced much disorder to the thin films, as judged by their lamella peak fwhm and  $\pi-\pi$  stacking peak fwhm shown in Table 3. Interestingly, the lamella spacing gradually decreases from 22.07, 21.96 to 21.75  $\text{\AA}$  for DPP-30, DPP-50, and DPP-70. This suggests alkyl chain interdigitates (packs) more tightly when the CBS ratio is increased in these polymers. On the other hand,  $\pi-\pi$  stacking distances is slightly enlarged.

AFM images and GIXRD patterns of DPP-100 by spin-coated and melt-processed thin films are shown in Figure 4. A striking difference is observed in AFM images. The melt-processed film forms condensed layered microstructures, while the spin-coated film exhibits loosely packed layers. The GIXRD patterns reveal considerably sharper peaks with a dramatically reduced peak width for the melt-processed film, suggesting that much larger domains and/or significantly improved ordering

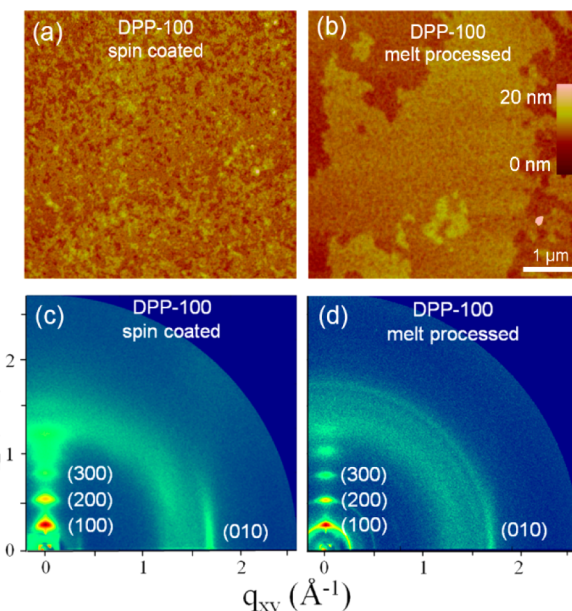


**Figure 4.** (a, b) AFM images for spin-coated and melt-processed DPP-100 film, respectively. (c, d) GIXRD patterns for spin-coated and melt-processed DPP-100 film, respectively.

existed in the melt-processed thin films. It is worth noting that such narrow peak widths ( $0.012\text{--}0.016 \text{\AA}^{-1}$ ) and large apparent domain sizes (40–50 nm) are not common among polymer materials. A similar observation is also found in the case of DPP-70. Both AFM and GIXRD results strongly support that melt-processed films have more ordered microstructures and packing motifs for charge transport than solution processed films, which is in good agreement with the OFET result that melt-processed devices displayed improved charge transport characteristics versus solution-processed devices.

Understanding how charge carriers move in the thin film is a critical step to design next generation semiconducting polymers. From Salleo's high molecular weight tie chain model<sup>23</sup> to Sirringhaus's disorder-free transport model,<sup>18</sup> there is much to investigate about charge transport in semiconducting polymer thin films. Our present study can provide some fresh insights into these charge transport models. For instance, DPP-100, having 100% flexible CBSs along the polymer backbone, obviously lacks intrachain charge transport pathways. Despite the presence of highly ordered  $\pi$ -stacks, the mobility from DPP-100 is about 2 orders of magnitude lower than that of DPP-0. This observation clearly underscores the importance of intrachain charge transport and a torsion-free polymer backbone as proposed in Sirringhaus's model. If a small amount of DPP-0 is blended into DPP-100 to serve as the tie chains, would charge transport in the blend film dramatically increase? Investigation of this question will be helpful to evaluate Salleo's model from a different angle.

## CONCLUSIONS

In summary, the modulation of electronic performance and solution processability in semiconducting polymers has been realized through introducing flexible conjugation-break spacers. This approach also opens a venue to design future high performance melt-processable semiconducting polymers. Importantly, melt-processed thin films present higher crystallinity and more ordered microstructures than their solution-

processed counterparts and hence offer substantially improved transport characteristics. These findings bode well for the development of low-cost melt-processed organic electronics via the industrially adapted extrusion and lamination process. Further efforts are needed to design melt-processable polymers with higher performance. Last, this approach also leads to a platform that is ideal for fundamental studies on charge transport. Ongoing work focuses on the influence of the flexible spacer length on charge transport as well as the tie-chain model.

## ■ ASSOCIATED CONTENT

### S Supporting Information

Materials, experimental details, NMR, TGA, DSC, AFM, GIXRD data, OFET characteristics, and device fabrication details. This material is available free of charge via the Internet at <http://pubs.acs.org>.

## ■ AUTHOR INFORMATION

### Corresponding Author

\*E-mail: [jgmei@purdue.edu](mailto:jgmei@purdue.edu) (J.M.).

### Notes

The authors declare no competing financial interest.

## ■ ACKNOWLEDGMENTS

The authors acknowledge the financial support from Purdue University. GIXRD measurements were carried out at the Stanford Synchrotron Radiation Laboratory, a national user facility operated by Stanford University on behalf of the U.S. Department of Energy, Office of Basic Energy Sciences. We thank Professor Bryan Boudouris for sharing instruments in his laboratory and Professor David McMillin and Professor Alexandra Azyner for helpful comments.

## ■ REFERENCES

- (1) Bao, Z.; Dodabalapur, A.; Lovinger, A. J. *J. Appl. Phys. Lett.* **1996**, *69*, 4108–4110.
- (2) Sirringhaus, H. *Adv. Mater.* **2014**, *26*, 1319–1335.
- (3) Meijer, E. J.; de Leeuw, D. M.; Setayesh, S.; van Veenendaal, E.; Huisman, B. H.; Blom, P. W. M.; Hummelen, J. C.; Scherf, U.; Klapwijk, T. M. *Nat. Mater.* **2003**, *2*, 678–682.
- (4) Arias, A. C.; MacKenzie, J. D.; McCulloch, I.; Rivnay, J.; Salleo, A. *Chem. Rev.* **2010**, *110*, 3–24.
- (5) Mei, J.; Diao, Y.; Appleton, A. L.; Fang, L.; Bao, Z. *J. Am. Chem. Soc.* **2013**, *135*, 6724–6746.
- (6) Sonar, P.; Singh, S. P.; Li, Y.; Soh, M. S.; Dodabalapur, A. *Adv. Mater.* **2010**, *22*, 5409.
- (7) Cheng, Y. J.; Yang, S. H.; Hsu, C. S. *Chem. Rev.* **2009**, *109*, 5868–5923.
- (8) Grimsdale, A. C.; Chan, K. L.; Martin, R. E.; Jokisz, P. G.; Holmes, A. B. *Chem. Rev.* **2009**, *109*, 897–1091.
- (9) Zhan, X. W.; Facchetti, A.; Barlow, S.; Marks, T. J.; Ratner, M. A.; Wasielewski, M. R.; Marder, S. R. *Adv. Mater.* **2011**, *23*, 268–284.
- (10) Tsao, H. N.; Cho, D. M.; Park, I.; Hansen, M. R.; Mavriniskiy, A.; Yoon, D. Y.; Graf, R.; Pisula, W.; Spiess, H. W.; Mullen, K. *J. Am. Chem. Soc.* **2011**, *133*, 2605–2612.
- (11) Zhao, Y.; Guo, Y.; Liu, Y. *Adv. Mater.* **2013**, *25*, 5372–5391.
- (12) Lei, T.; Dou, J. H.; Pei, J. *Adv. Mater.* **2012**, *24*, 6457–6461.
- (13) Beaujuge, P. M.; Amb, C. M.; Reynolds, J. R. *Acc. Chem. Res.* **2010**, *43*, 1396–1407.
- (14) Facchetti, A. *Chem. Mater.* **2011**, *23*, 733–758.
- (15) Wang, C.; Dong, H.; Hu, W.; Liu, Y.; Zhu, D. *Chem. Rev.* **2012**, *112*, 2208–67.
- (16) Gasperini, A.; Bivaud, S.; Sivula, K. *Chem. Sci.* **2014**, *5*, 4922–4927.
- (17) Martens, H. C. F.; Blom, P. W. M.; Schoo, H. F. M. *Phys. Rev. B* **2000**, *61*, 7489–7493.
- (18) Venkateshvaran, D.; Nikolla, M.; Sadhanala, A.; Lemaur, V.; Zelazny, M.; Kepa, M.; Hurhangee, M.; Kronemeijer, A. J.; Pecunia, V.; Nasrallah, I.; Romanov, I.; Broch, K.; McCulloch, I.; Emin, D.; Olivier, Y.; Cornil, J.; Beljonne, D.; Sirringhaus, H. *Nature* **2014**, *515*, 384–388.
- (19) Lee, H. K. H.; Li, Z.; Constantinou, I.; So, F.; Tsang, S. W.; So, S. K. *Adv. Energy Mater.* **2014**, *4*, 1400768.
- (20) Yiu, A. T.; Beaujuge, P. M.; Lee, O. P.; Woo, C. H.; Toney, M. F.; Frechet, J. M. J. *J. Am. Chem. Soc.* **2012**, *134*, 2180–2185.
- (21) Mei, J.; Bao, Z. *Chem. Mater.* **2014**, *26*, 604–615.
- (22) Sirringhaus, H. *Adv. Mater.* **2005**, *17*, 2411–2425.
- (23) Noriega, R.; Rivnay, J.; Vandewal, K.; Koch, F. P. V.; Stingelin, N.; Smith, P.; Toney, M. F.; Salleo, A. *Nat. Mater.* **2013**, *12*, 1038–1044.
- (24) Tsao, H. N.; Mullen, K. *Chem. Soc. Rev.* **2010**, *39*, 2372–86.
- (25) Nielsen, C. B.; Turbiez, M.; McCulloch, I. *Adv. Mater.* **2013**, *25*, 1859–1880.
- (26) Chen, S. Y.; Sun, B.; Hong, W.; Aziz, H.; Meng, Y.; Li, Y. N. *J. Mater. Chem. C* **2014**, *2*, 2183–2190.
- (27) Flory, P. J. *Principles of Polymer Chemistry*; Cornell University Press: Ithaca, NY, 1953.
- (28) Mondal, R.; Ko, S.; Norton, J. E.; Miyaki, N.; Becerril, H. A.; Verploegen, E.; Toney, M. F.; Bredas, J.-L.; McGehee, M. D.; Bao, Z. *J. Mater. Chem.* **2009**, *19*, 7195–7197.
- (29) Rivnay, J.; Mannsfeld, S. C. B.; Miller, C. E.; Salleo, A.; Toney, M. F. *Chem. Rev.* **2012**, *112*, 5488–5519.